Received: 17 February 2021 | Revised: 27 May 2021 | Accepted: 31 May 2021

DOI: 10.1002/aoc.6343

FULL PAPER

Applied Organometallic Chemistry WILEY

Organoruthenium (II) complexes featuring pyrazole-linked thiosemicarbazone ligands: Synthesis, DNA/BSA interactions, molecular docking, and cytotoxicity studies

Priyanka Khanvilkar[1] | **Soumya R. Dash**[2] | **Devjani Banerjee**[3] | **Aliasgar Vohra**[4] | **Ranjitsinh Devkar**[4] | **Debjani Chakraborty**[1]

[1]Department of Chemistry, The Maharaja Sayajirao University of Baroda, Vadodara, India

[2]Physical and Material Chemistry Division, CSIR-NCL Pune, Pune, India

[3]Cell and Molecular Biology Division, The Maharaja Sayajirao University of Baroda, Vadodara, India

[4]Department of Zoology, The Maharaja Sayajirao University of Baroda, Vadodara, India

Correspondence
Debjani Chakraborty, Department of Chemistry, Faculty of Science, The M S University of Baroda, Vadodara, India.
Email: debjani.chakraborty-chem@msubaroda.ac.in

Funding information
DST-PURSE, Grant/Award Number: FS/206/19-20; RFSMS-BSR, Grant/Award Number: F.5-71/2007(BSR); University Grants Commission, Grant/Award Number: UGC F.No. 43-238/2014(SR)

Abstract

A series of pyrazol-derived thiosemicarbazone ligands (**L1**–**L4**) were synthesized and reacted with $[Ru(p\text{-cymene})(\mu\text{-}Cl)Cl]_2$ to yield a series of "piano-stool"-type binuclear ruthenium (II)–arene-thiosemicarbazone complexes (**C1**–**C8**) of the general type $[(Ru(\eta^6\text{-}p\text{-cym})L)_2(\mu\text{-im/azpy})]\ Cl_{1-2}$ (L = diphenylpyrazole thiosemicarbazone; cym = p-cymene; im = imidazole; azpy = 4,4′-azopyridine). The thiosemicarbazone ligands act as N and S donors binding to the Ru(II) center via the imine nitrogen and the thione sulfur atoms. The complexes were characterized by NMR, FTIR, UV–Vis spectroscopy, and ESI^+ mass spectrometry. The binding of the complexes to calf thymus deoxyribonucleic acid (CT-DNA) and bovine serum albumin (BSA) was evaluated, and it has been established that the binuclear complexes have good binding efficacies with DNA ($K_b = 10^4$–$10^5\ M^{-1}$) and BSA ($K_a = 10^5$–$10^6\ M^{-1}$). This is attributed to the arene moieties present in the ligands of the complexes that can have hydrophobic interactions with DNA/BSA. Ethidium bromide (EB) displacement studies and DNA viscosity measurements revealed intercalative interaction of the complexes with DNA. Static interaction of the complexes with BSA was revealed by fluorescence quenching studies. Molecular docking studies confirmed base stacking, H-bonding, and hydrophobic interactions with the biomolecules. In vitro antiproliferative studies of the complexes affirmed that the complexes are cytotoxic towards the HeLa (human cervical cancer) cell line with IC_{50} values in range of 17.3–41.3 μM.

KEYWORDS

binuclear ruthenium (II) complexes, DNA/BSA binding interactions, HeLa human cervical carcinoma, pyrazole-derived thiosemicarbazone

1 | INTRODUCTION

Pyrazoles represent an important pharmacophore with diverse biological activities, and some derivatives are already in use as drugs for therapeutic purposes. Therefore, their design and synthesis is an important field of research. Modification of the substituents at positions 1, 3, and 5 has resulted into new pyrazole derivatives with wide spectrum

biological activities. Structural changes at the different positions of the basic molecule results in better pharmacological activities, providing it with antimicrobial, anticonvulsant, analgesic, anti-inflammatory, antiviral, antimalarial, and anticancer properties. Pyrazole-pyrimidine derivatives have shown antiproliferative activity against NCl-H226 (human lung carcinoma), NPC-TW01 (nasopharyngeal cancer), T-cell leukemia (Jurkat) cells, and a group of other human cancer cell lines.[1–3] A series of pyrazole–sulfonamide conjugates with antiproliferative activity against HeLa and C6 cell lines was reported by Mert et al.[4] Via et al. reported antiproliferative activities of benzothiopyranopyrazole derivatives exerted on HeLa and HL-60 cells.[5] A phenyl, *p*-chlorophenyl, or *p*-methoxyphenyl substituent at 1-position and a methoxy substituent at the 7-position of the heterocyclic moiety was found to be responsible for the activities.

In vitro antiproliferative activities of a series of functionally substituted pyrazoles, on a panel of 60 cell lines was investigated by Nitulescu et al.[6] *N*-benzoyl-*N*′-(3-(4-bromophenyl)-1*H*-pyrazol-5-yl)-thiourea showed promising results. Prasad et al.[7] investigated novel 4,5-dihydropyrazole derivatives that were found to be more effective than *cis*-platin. The derivative with an electron-withdrawing chloro group in the 4-position of the lipophilic heterocycle exhibited high anticancer activity ($IC_{50} = 4.94$ mM) against HeLa cell lines. Rai et al. reported the synthesis and anticancer activity of a series of pyrazole chalcones against MCF-7 and HeLa cell lines.[8] The 4-fluoro-phenyl and 5-fluoro-pyridine derivatives showed the highest inhibition in human MCF-7 and HeLa cell lines. Two comprehensive reviews by Ansari et al.[9] and Karrouchi et al.[10] highlight the different synthesis methods and the pharmacological properties of pyrazole derivatives developed by many researchers around the globe.

Thiosemicarbazones (TSCs) are well known for their versatility and various pharmacological properties including anticancer activity. Heterocyclic thiosemicarbazones have gained considerable interest in medicinal chemistry due to their ability to diffuse through the semipermeable membrane of the cell lines. They show a range of biological activities including antitubercular, antibacterial, antimalarial, antileprosy, antiparasitic, antineoplastic, antiviral, antiproliferative, antioxidant, and antitumor activities.[11]

Thiosemicarbazones (TSCs) are inhibitors of the iron containing enzyme ribonucleotide reductase, which catalyzes the conversion of ribonucleotides to 2′-deoxyribonucleotides and hence is essential for DNA synthesis and repair.[12] The first discovered representative of this class of compounds was 2-formylpyridine thiosemicarbazone that exhibited potent anticancer activity. Another well-known representative of this family, triapine (3-aminopyridine-2-carboxaldehyde thiosemicarbazone), was extensively investigated in numerous clinical phase I and II trials in mono or combination therapies. Ribonucleotide reductases are the primary cellular target of Triapine. The TSCs, *N*′-(6,7-dihydroquinolin-8(5*H*)-ylidene)-4-(pyridin-2-yl)piperazine-1-carbothiohydrazide (COTI-2), and di-2-pyridylketone-4-cyclohexyl-4-methyl-3-thiosemicarbazone (DpC) have entered the human clinical trials, renewing interest in this class of therapeutically useful compounds.[12,13]

It was observed that tethering two different biologically active moieties can bestow the resulting compound with new biological properties.[14] A conjugation of TSC and pyrazol derivatives can result into a potent component for anticancer and other therapeutic drugs. In addition, biological properties of thiosemicarbazones have been found to be augmented by coordination to the metal ions.[15,16] This approach was utilized by combining the Ru–arene fragment to thiosemicarbazones.[17]

The piano-stool-type Ru(II)-arene-based compounds are envisaged as potential and compelling candidates for cancer treatment.[18,19] The arene moiety provides significant pharmacological properties to the complexes, namely, impact in cellular uptake, enhanced hydrophobicity, and biomolecular recognition process leading to improved passive transport across the cell membrane. It is evident that the interaction of metal complexes with DNA or protein is enhanced due to the π-stacking of the arene ligand that explains their biological activity and various pharmacological properties.[20]

The dicyanamidobenzene-bridged diruthenium complex $[\{Ru(tpy)(thd)\}_2(\mu\text{-dicyd})][PF_6]$ {dicyd = 1,4-dicyanamidobenzene, tpy = 2,2′:6′,2″-terpyridine, thd = 2,2,6,6-tetramethyl-3,5-heptanedione} was synthesized and characterized by X-ray crystallography.[21] XRD studies of the binuclear Ru(II)-arene-triphenylphosphine complex with terephthalic acid as bridging ligand were carried by Honorato et al. The bidentate O–O coordination mode of the carboxylate groups was unambiguously confirmed by the X-ray technique.[22]

This paper reports the design, synthesis, and biological investigation of novel binuclear ruthenium (II)-arene complexes (**C1**–**C8**) containing pyrazole substituted thiosemicarbazone ligands (**L1**–**L4**).

2 | EXPERIMENTAL SECTION

2.1 | Materials and instrumentation

The chemicals and solvents used for synthesis and characterization of the complexes were of analytical grade. Pyrazole carboxaldehyde was purchased from

Sigma-Aldrich; Thiosemicarbazide was purchased from SRL (Sisco Research Laboratory, Mumbai, India). The precursor $[Ru(\eta^6\text{-}p\text{-cymene})Cl_2]_2$ was prepared according to the procedure cited in literature.[23,24] CT-DNA, trisodium citrate, and EB (ethidium bromide) were purchased from SRL (Sisco Research Laboratory, Mumbai, India). $RuCl_3{\cdot}3H_2O$ and BSA (bovine serum albumin) were purchased from Hi-media. HeLa cell line was obtained from National Centre for Cell Science (NCCS), Pune, India. ESI mass spectra of the complexes were recorded on Applied Biosystem API 2000 Mass spectrometer. Infrared spectra (400–4000 cm^{-1}) were recorded on α-Bruker FTIR with samples prepared as KBr pellets. ^1H NMR spectra were recorded on a Bruker AR X 400 Spectrometer at 400 MHz using DMSO as solvent. C, H, and N elemental analysis were performed on a PerkinElmer 240B elemental analyzer. UV spectra were recorded in DMSO solution at concentrations in the range 10^{-6}–10^{-3} M on Perkin Elmer Lambda-35 dual beam UV–Vis spectrophotometer. Fluorescence spectra were recorded in solution on JASCO FP-6300 fluorescence spectrophotometer. To evaluate the data obtained from DNA/BSA interaction (titration) experiments, the OriginPro 8 software was employed. ORCA program package (version 4.0.1.2) was used for geometry optimization.

2.2 | General procedure for the preparation of pyrazol thiosemicarbazones (L1–L4)

The ligands were synthesized and characterized according to the literature (Scheme 1).[25] In brief, an equimolar amount of a substituted thiosemicarbazide (0.01 M) and 1,3-diphenyl-1*H*-pyrazole-4-carboxaldehyde (0.01 M) in methanol with a small amount of glacial acetic acid added was refluxed for 10 h. The progress of the reaction was monitored by TLC. After completion of the reaction, the mixture was poured into crushed ice; the separated product was filtered off, washed with cold methanol, and dried under vacuum. The ligands were recrystallized in methanol, and pure white crystalline product was obtained. The yield and spectral data of ligands are discussed below.

2.2.1 | 1-((1,3-Diphenyl-1*H*-pyrazol-4-yl) methylene)thiosemicarbazone (**L1**)

L1 was synthesized by condensation reaction of thiosemicarbazide (2 mmol, 183 mg) and 1,3-diphenyl-1*H*-pyrazole-4-carboxaldehyde (2 mmol, 498 mg). Solubility: MeOH, DMSO, DMF; yield 79.6%; molecular weight 321.4 g/mol; molecular formula $C_{17}H_{15}N_5S$; color: white; anal.: found: C, 63.27; H, 4.32; N, 21.39. Calc.: C, 63.53; H, 4.70; N, 21.79; MS *m/z*: obs (calc): 322.2 (321.4) ($M^+ + 1$); ^1H-NMR (DMSO-d_6): δppm 7.37, (tri, 1H, Ar–H); 7.42–7.51, (m, 5H, Ar–H); 7.77, (d, 2H, $J = 6.8$ Hz, Ar–H); 7.28, (s, 1H, Ar–H); 7.79, (d, 2H, $J = 7.6$ Hz, Ar–H); 8.03, 7.79 (s, 2H, NH_2); 8.36 (s, 1H, HC=N); 10.07, (s, 1H, N–NH); IR (KBr, cm^{-1}): $\nu_{(Ar)C-H}$ 2883, $\nu_{(NNH)}$ 3434; $\nu_{(NH2)}$ 3356, 3280; $\nu_{(C=N)}$ 1599; $\nu_{(N-N)}$ 1053; $\nu_{(C=S)assym}$ 1291; $\nu_{(C=S)sym}$ 816.

2.2.2 | 1-((1,3-Diphenyl-1*H*-pyrazol-4-yl) methylene)-4-methyl-3-thiosemicarbazone (**L2**)

Prepared by condensation of 4-methyl-3-thiosemicarbazide (1.9 mmol, 200 mg) and 1,3-diphenyl-1*H*-pyrazole-

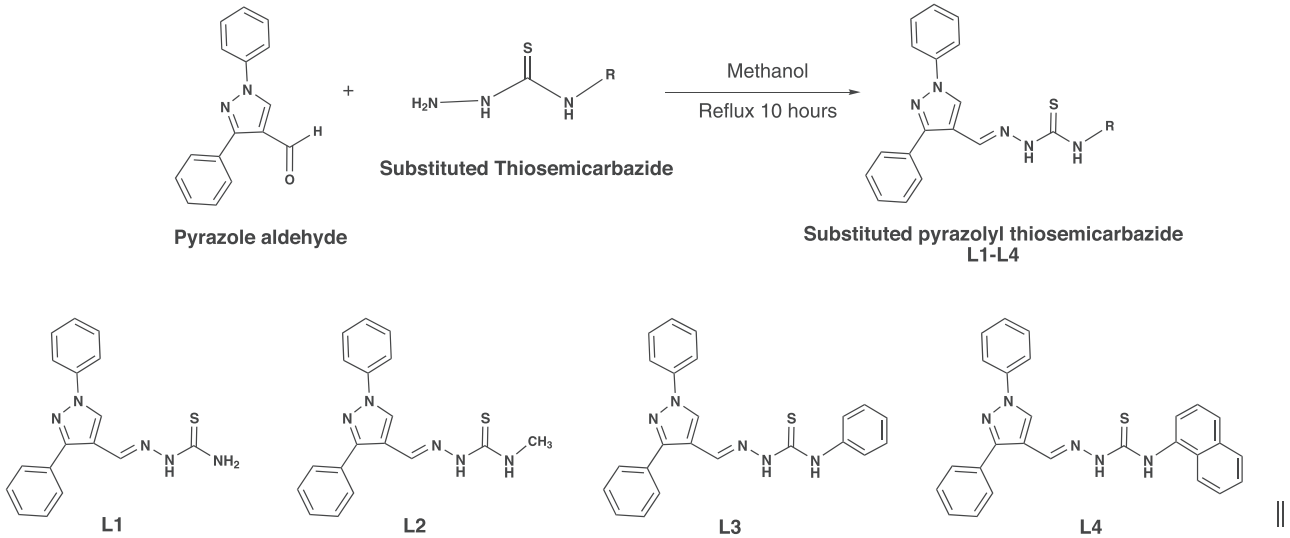

SCHEME 1 General synthetic route to diphenyl pyrazol thiosemicarbazones **L1**–**L4**

4-carboxaldehyde (1.9 mmol, 472 mg). Solubility: MeOH, DMSO, DMF; yield 80.4%; molecular weight 335.4 g/mol; molecular formula $C_{18}H_{17}N_5S$; color: pale yellow; anal.: found: C, 64.11; H, 4.72; N, 20.51. Calc.: C, 64.45; H, 5.11; N, 20.88; MS *m/z*: obs (calc): 337.1 (335.4) ($M^+ + 2$); ^{1}H-NMR (DMSO-d_6): δppm 7.47, (tri, 1H, Ar–H); 7.49–7.59, (m, 5H, Ar–H); 7.69, (d, 2H, $J = 6.8$ Hz, Ar–H); 8.22, (s, 1H, Ar–H); 7.91, (d, 2H, $J = 7.6$ Hz, Ar–H); 8.28, (s, 1H, NH–CH_3); 3.03, (s, 3H, N–CH_3); 9.08 (s, 1H, HC=N); 11.41 (s, 1H, N–NH); IR (KBr, cm^{-1}): $\nu_{(Ar)C-H}$ 2932, $\nu_{(NN-H)}$ 3389; $\nu_{(NH-CH3)}$ 3325; $\nu_{(C=N)}$ 1598; $\nu_{(N-N)}$ 1054; $\nu_{(C=S)assym}$ 1266; $\nu_{(C=S)sym}$ 823.

2.2.3 | 1-((1,3-Diphenyl-1*H*-pyrazol-4-yl) methylene)-4-phenyl-3-thiosemicarbazone (**L3**)

Condensation of 4-phenyl-3-thiosemicarbazide (2.9 mmol, 500 mg) and 1,3-diphenyl-1*H*-pyrazole-4-carboxaldehyde (2.9 mmol, 742 mg) yielded **L3**. Solubility: MeOH, DMSO, DMF; yield 81.06%; molecular weight 397.5 g/mol; molecular formula $C_{23}H_{19}N_5S$; color: whitish yellow; anal.: found: C, 69.10; H, 4.47; N, 17.39. Calc.: C, 69.50; H, 4.82; N, 17.62; MS *m/z*: obs (calc): 398.1 (397.5) ($M^+ + 1$); ^{1}H-NMR (DMSO-d_6): δppm 7.38, (tri, 1H, Ar–H); 7.50–7.58, (m, 5H, Ar–H); 7.72, (d, 2H, $J = 6.7$ Hz, Ar–H); 8.34, (s, 1H, Ar–H); 7.92, (d, 2H, $J = 7.4$ Hz, Ar–H); 7.21–7.49, (5H, m, N–C_6H_5); 9.86, (s, 1H, NH–C_6H_5); 9.27, (s, 1H, HC=N); 11.77, (s, 1H, N–NH); IR (KBr, cm^{-1}): $\nu_{(Ar)C-H}$ 2964; $\nu_{(NN-H)}$ 3335; $\nu_{(NH-C6H5)}$ 3290; $\nu_{(C=N)}$ 1597; $\nu_{(N-N)}$ 1065; $\nu_{(C=S)assym}$ 1268; $\nu_{(C=S)sym}$ 824.

2.2.4 | 1-((1,3-Diphenyl-1*H*-pyrazol-4-yl) methylene)-4-(naphthalen-1-yl)-3-thiosemicarbazone (**L4**)

The synthesis of **L4** was carried out by condensation of 4-(1-naphthyl)-3-thiosemicarbazide (1.6 mmol, 350 mg) and 1,3-diphenyl-1*H*-pyrazole-4-carboxaldehyde (1.6 mmol, 399 mg). Solubility: MeOH, DMSO, DMF; yield 85.4%; molecular weight 447.2 g/mol; molecular formula $C_{27}H_{21}N_5S$; color: yellow; anal.: found: C, 72.22; H, 4.38; N, 15.41. Calc.: C, 72.46; H, 4.73; N, 15.65; MS *m/z*: obs (calc): 448.1 (447.2) ($M^+ + 1$); ^{1}H-NMR (DMSO-d_6): δppm 7.34, (tri, 1H, Ar–H); 7.56–7.58, (m, 5H, Ar–H); 7.75, (d, 2H, $J = 6.8$ Hz, Ar–H); 7.75, (s, 1H, Ar–H); 7.88, (d, 2H, $J = 8.6$ Hz, Ar–H); 7.46–7.56, (7H, m, N–$C_{10}H_7$); 10.17, (s, 1H, NH–$C_{10}H_7$); 9.26, (s, 1H, HC=N); 11.88, (s, 1H, N–NH); IR (KBr, cm^{-1}): $\nu_{(Ar)C-H}$ 2971; $\nu_{(NN-H)}$ 3334; $\nu_{(NH-C10H7)}$ 3123; $\nu_{(C=N)}$ 1597; $\nu_{(N-N)}$ 1047; $\nu_{(C=S)assym}$ 1276; $\nu_{(C=S)sym}$ 807.

2.3 | General synthetic procedure of $[(Ru(\eta^6\text{-}p\text{-cym})L)_2(\mu\text{-im/azpy})]Cl_{1-2}$ complexes: (C1–C8)

The ligand **L** in 2.5-ml methanol was added to a solution of $[Ru(\eta^6\text{-}p\text{-cymene})Cl_2]_2$ in 2.5-ml CH_2Cl_2 in the molar ratio 2:1, and the reaction mixture was stirred overnight at room temperature. Slow evaporation of the solution yielded the reddish brown mononuclear complex $[Ru(\eta^6\text{-}p\text{-cym})(L)]Cl$, which was filtered, washed with pet ether and CH_2Cl_2, and dried. The bridging ligand imidazole or 4,4′-azopyridine was added to the mononuclear complex dissolved in a mixture of 5 ml of CH_2Cl_2 and 3 ml of CH_3OH in 1:2 ratios. To deprotonate the ring –NH, 1.0-M NaOH solution was added after addition of the imidazole ligand.[26] The solution was stirred for 24 h at room temperature under N_2 atmosphere. The reddish brown solid obtained was filtered, washed with pet ether, and dried in oven at 40°C for 1 h. The complexes so obtained were recrystallized from dichloromethane and ether. Scheme 2 shows the general synthetic route for preparation of the complexes.

2.4 | Chemical characterization data of the complexes

2.4.1 | $[(Ru(\eta^6\text{-}p\text{-cym})L1)_2(\mu\text{-im})]Cl$ (**C1**)

Yield: 62.9%; molecular weight 1214.9 g/mol; molecular formula $C_{57}H_{60}ClN_{12}Ru_2S_2$; anal.: found: C, 55.99; H, 4.78; N, 13.77. Calc.: C, 56.36; H, 4.98; N, 13.84. ESI-MS *m/z*: obs (calc): 1179.27 (1179.5) (M^+); δ_H (400 MHz, DMSO-d_6) 7.38, (tri, 1H, Ar–H); 7.55, (m, 5H, Ar–H); 7.69, (d, 2H, $J = 6.8$ Hz, Ar–H); 7.77, (s, 1H, Ar–H); 7.83, (d, 2H, $J = 7.6$ Hz, Ar–H); 8.22, (s, 2H, NH_2); 8.69, (s, 1H, HC=N); 5.82–5.77; (m, 4H, *p*-cym Ar–H); 2.84–2.50, (q, 1H, *p*-cym-*iso*-prop-CH); 1.97, (s, 3H, *p*-cym Ar–CH_3); 1.05, (d, 6H, *p*-cym-*iso*-prop-$(CH_3)_2$); 7.93 (d, 2H, imidazole CH=CH); FTIR (KBr/cm^{-1}): $\nu_{(Ar)C-H}$ 2959, $\nu_{(NH2)}$ 3050, $\nu_{(C=N)}$ 1588, $\nu_{(C-S)sym}$ 770; Λ_M ($\Omega^{-1}\cdot m^2\cdot M^{-1}$) 75.

2.4.2 | $[(Ru(\eta^6\text{-}p\text{-cym})L2)_2(\mu\text{-im})]Cl$ (**C2**)

Yield: 77.5%; molecular weight 1243.0 g/mol; molecular formula $C_{59}H_{64}ClN_{12}Ru_2S_2$; anal. found: C, 56.61; H, 4.89; N, 13.17. Calc.: C, 57.01; H, 5.19; N, 13.52. ESI-MS *m/z*: obs (calc): 1207.7 (1207.5) (M^+); δ_H (400 MHz, DMSO-d_6) 7.50, (tri, 1H, Ar–H); 7.59, (m, 5H, Ar–H); 7.68, (d, 2H, $J = 6.8$ Hz, Ar–H); 7.79, (s, 1H, Ar–H); 7.80, (d, 2H, $J = 7.6$ Hz, Ar–H); 7.92, (s, 1H, NH–CH_3); 8.22, (s, 1H, HC=N); 5.82–5.73, (m, 4H, *p*-cym Ar–H);

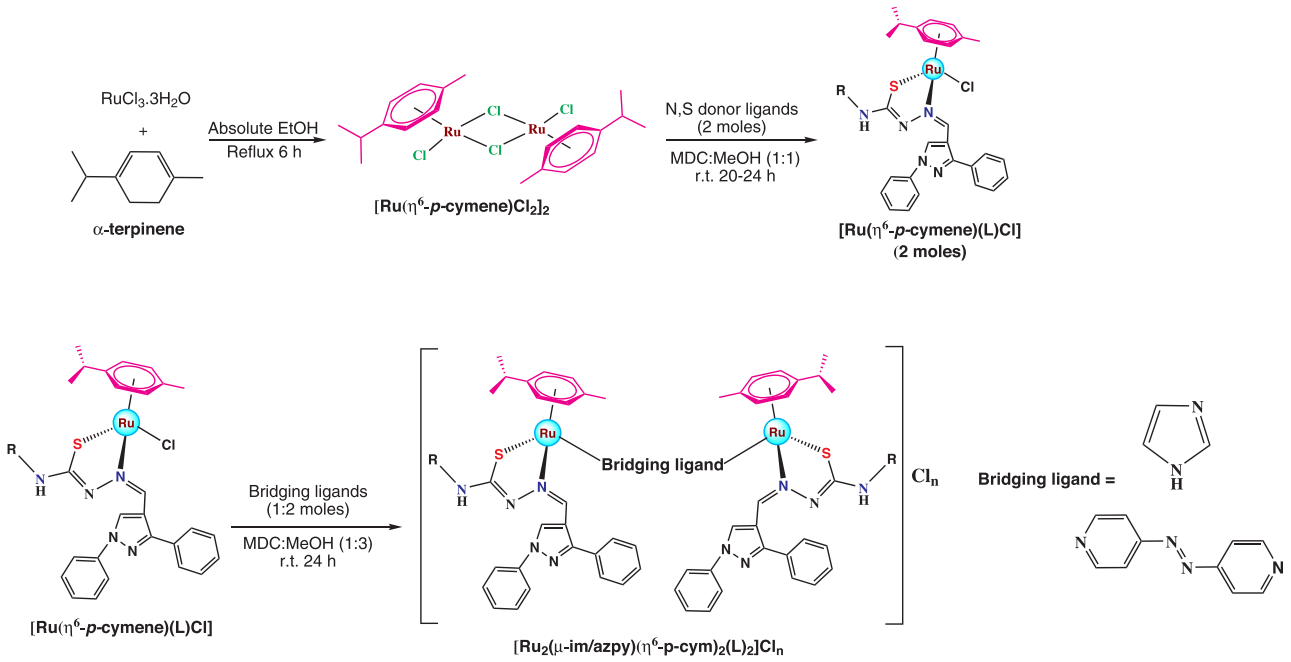

SCHEME 2 General synthetic route to complexes **C1**–**C8**, $n = 1, 2$ and R = H, CH_3, C_6H_5, $C_{10}H_7$

2.95–2.49, (q, 1H, *p*-cym-*iso*-prop-CH); 1.98, (s, 3H, *p*-cym Ar–CH_3); 1.02, (d, 6H, *p*-cym-*iso*-prop-$(CH_3)_2$); 7.92, (d, 2H, imidazole CH=CH); FTIR (KBr/cm^{-1}): $\nu_{(Ar)\,C-H}$ 2962, $\nu_{(NH-CH3)}$ 3124, $\nu_{(C=N)}$ 1597, $\nu_{(C-S)sym}$ 748; Λ_M ($\Omega^{-1}\cdot m^2\cdot M^{-1}$) 72.

2.4.3 | [(Ru(η⁶-*p*-cym)L3)$_2$(μ-im)]Cl (**C3**)

Yield: 48.4%; molecular weight 1367.1 g/mol; molecular formula $C_{69}H_{68}ClN_{12}Ru_2S_2$; anal.: found: C, 60.12; H, 4.89; N, 11.98. Calc.: C, 60.62; H, 5.01; N, 12.29. ESI-MS *m/z*: obs (calc): 1330.3 (1331.1) ($M^+ - 1$); δ_H (400 MHz, DMSO-d_6) 7.38, (tri, 1H, Ar–H); 7.53, (m, 5H, Ar–H); 7.64, (d, 2H, $J = 6.8$ Hz, Ar–H); 7.79, (s, 1H, Ar–H); 7.82, (d, 2H, $J = 7.6$ Hz, Ar–H); 8.10, (s, 1H, NH–C_6H_5); 8.34, (s, 1H, HC=N); 5.81–5.50, (m, 4H, *p*-cym Ar–H); 2.50–2.24, (q, 1H, *p*-cym-*iso*-prop-CH); 2.15, (s, 3H, *p*-cym Ar–CH_3); 1.15, (d, 6H, *p*-cym-*iso*-prop-$(CH_3)_2$); 7.82, (d, 2H, imidazole CH=CH); FTIR (KBr/cm^{-1}): $\nu_{(Ar)\,C-H}$ 2970, $\nu_{(NH-C6H5)}$ 3163, $\nu_{(C=N)}$ 1589, $\nu_{(C-S)sym}$ 756; Λ_M ($\Omega^{-1}\cdot m^2\cdot M^{-1}$) 76.

2.4.4 | [(Ru(η⁶-*p*-cym)L4)$_2$(μ-im)]Cl (**C4**)

Yield: 58.7%; molecular weight 1467.3 g/mol; molecular formula $C_{77}H_{72}ClN_{12}Ru_2S_2$; anal.: found: C, 62.98; H, 3.79; N, 11.86. Calc.: C, 63.03; H, 4.95; N, 11.46. ESI-MS *m/z*: obs (calc): 1433.2 (1431.4) ($M^+ + 1$); δ_H (400 MHz, DMSO-d_6) 7.37, (tri, 1H, Ar–H); 7.55, (m, 5H, Ar–H); 7.63, (d, 2H, $J = 6.8$ Hz, Ar–H); 7.65, (s, 1H, Ar–H); 7.81, (d, 2H, $J = 7.6$ Hz, Ar–H); 7.75, (s, 1H, NH–$C_{10}H_7$); 8.32, (s, 1H, HC=N); 6.68–5.92, (m, 4H, *p*-cym Ar–H), 3.93–3.35, (q, 1H, *p*-cym-*iso*-prop-CH); 2.49, (s, 3H, *p*-cym Ar–CH_3); 1.93, (d, 6H, *p*-cym-*iso*-prop-$(CH_3)_2$); 7.75, (d, 2H, imidazole CH=CH); FTIR (KBr/cm^{-1}): $\nu_{(Ar)\,C-H}$ 2959, $\nu_{(NH-C10H7)}$ 3138, $\nu_{(C=N)}$ 1595, $\nu_{(C-S)sym}$ 775; Λ_M ($\Omega^{-1}\cdot m^2\cdot M^{-1}$) 70.

2.4.5 | [(Ru(η⁶-*p*-cym)L1)$_2$(μ-azpy)]Cl$_2$ (**C5**)

Yield: 61.7%; molecular weight 1366.6 g/mol; molecular formula $C_{64}H_{64}Cl_2N_{14}Ru_2S_2$; anal.: C, 58.99; H, 4.73; N, 15.07. Calc.: C, 59.33; H, 4.98; N, 15.14. ESI-MS *m/z*: obs (calc): 644.8 (645.7) ($M^{2+} - 1$); δ_H (400 MHz, DMSO-d_6) 7.06, (tri, 1H, Ar–H); 7.10, (m, 5H, Ar–H); 7.12, (d, 2H, $J = 6.8$ Hz, Ar–H); 7.81, (s, 1H, Ar–H); 7.84, (d, 2H, $J = 7.6$ Hz, Ar–H); 8.18, (s, 2H, NH_2); 8.21, (s, 1H, HC=N); 6.84–6.79, (m, 4H, *p*-cym Ar–H); 3.16–2.24, (q, 1H, *p*-cym-*iso*-prop-CH); 1.75, (s, 3H, *p*-cym Ar–CH_3); 1.15, (d, 6H, *p*-cym-*iso*-prop-$(CH_3)_2$); FTIR (KBr/cm^{-1}): $\nu_{(Ar)C-H}$ 2961, $\nu_{(NH2)}$ 3159, $\nu_{(C=N)}$ 1589, $\nu_{(C-S)sym}$ 761, $\nu_{N=N}$ 1408; Λ_M ($\Omega^{-1}\cdot m^2\cdot M^{-1}$) 134.

2.4.6 | $[(Ru(\eta^6\text{-}p\text{-cym})L2)_2(\mu\text{-azpy})]Cl_2$ (**C6**)

Yield: 78.8%; molecular weight 1394.6 g/mol; molecular formula $C_{66}H_{68}Cl_2N_{14}Ru_2S_2$; anal.: C, 59.52; H, 4.87; N, 14.56. Calc.: C, 59.89; H, 5.18; N, 14.82, ESI-MS *m/z*: obs (calc): 660.3 (661.2) ($M^{2+} - 1$); δ_H (400 MHz, DMSO-d_6) 7.33, (tri, 1H, Ar–H); 7.36, (m, 5H, Ar–H); 7.77, (d, 2H, $J = 6.8$ Hz, Ar–H); 7.79, (s, 1H, Ar–H); 7.81, (d, 2H, $J = 7.6$ Hz, Ar–H); 8.44, (s, 1H, NH–CH_3); 8.46, (s, 1H, HC=N); 5.82–5.77, (m, 4H, *p*-cym Ar–H); 3.35–2.86, (q, 1H, *p*-cym-*iso*-prop-CH); 1.97, (s, 3H, *p*-cym Ar–CH_3); 1.17, (d, 6H, *p*-cym-*iso*-prop-$(CH_3)_2$); FTIR (KBr/cm^{-1}): $\nu_{(Ar)C-H}$ 2960, $\nu_{(NH-CH3)}$ 3162, $\nu_{(C=N)}$ 1588, $\nu_{(C-S)sym}$ 764, $\nu_{N=N}$ 1402; Λ_M ($\Omega^{-1}\cdot m^2\cdot M^{-1}$) 135.

2.4.7 | $[(Ru(\eta^6\text{-}p\text{-cym})L3)_2(\mu\text{-azpy})]Cl_2$ (**C7**)

Yield: 89.7%; molecular weight 1518.8 g/mol; molecular formula $C_{76}H_{72}Cl_2N_{14}Ru_2S_2$; anal.: C, 62.73; H, 4.67; N, 13.16. Calc.: C, 63.05; H, 5.01; N, 13.54, ESI-MS *m/z*: obs (calc): 724.2 (723.9) (M^{2+}); δ_H (400 MHz, DMSO-d_6) 7.36, (tri, 1H, Ar-H); 7.63, (m, 5H, Ar–H); 7.72, (d, 2H, $J = 6.8$ Hz, Ar–H); 7.42, (s, 1H, Ar–H); 7.64, (d, 2H, $J = 7.6$ Hz, Ar–H); 8.24, (s, 1H, NH–C_6H_5); 8.45, (s, 1H, HC=N); 5.49–5.44, (m, 4H, *p*-cym Ar–H); 2.24–2.17, (q, 1H, *p*-cym-*iso*-prop-CH); 1.91, (s, 3H, *p*-cym Ar–CH_3); 1.03, (d, 6H, *p*-cym-*iso*-prop-$(CH_3)_2$); FTIR (KBr/cm^{-1}): $\nu_{(Ar)C-H}$ 2960, $\nu_{(NH-C6H5)}$ 3045, $\nu_{(C=N)}$ 1590, $\nu_{(C=S)sym}$ 753, $\nu_{N=N}$ 1404; Λ_M ($\Omega^{-1}\cdot m^2\cdot M^{-1}$) 133.

2.4.8 | $[(Ru(\eta^6\text{-}p\text{-cym})L4)_2(\mu\text{-azpy})]Cl_2$ (**C8**)

Yield: 89.3%; molecular weight 1618.9 g/mol; molecular formula $C_{84}H_{76}Cl_2N_{14}Ru_2S_2$; anal.: C, 64.79; H, 4.55; N, 12.42. Calc.: C, 65.18; H, 4.95; N, 12.67. ESI-MS *m/z*: obs (calc): 772.2 (773.2) ($M^{2+} - 1$); δ_H (400 MHz, DMSO-d_6) 7.38, (tri, 1H, Ar–H); 7.44, (m, 5H, Ar–H); 7.70, (d, 2H, $J = 6.8$ Hz, Ar–H); 7.78, (s, 1H, Ar–H); 7.99, (d, 2H, $J = 7.6$ Hz, Ar–H); 8.23, (s, 1H, NH–$C_{10}H_7$); 8.57, (s, 1H, HC=N); 7.01–6.99, (m, 4H, *p*-cym Ar–H); 2.51–2.49, (q, 1H, *p*-cym-*iso*-prop-CH); 1.97, (s, 3H, *p*-cym Ar–CH_3); 1.02, (d, 6H, *p*-cym-*iso*-prop-$(CH_3)_2$); FTIR (KBr/cm^{-1}): $\nu_{(Ar)C-H}$ 2959, $\nu_{(NH-C10H7)}$ 3161, $\nu_{(C=N)}$ 1593, $\nu_{(C=S)sym}$ 775, $\nu_{N=N}$ 1431; Λ_M ($\Omega^{-1}\cdot m^2\cdot M^{-1}$) 131.

2.5 | Geometry optimization

All DFT calculations were performed by using the b-p functional[27] and def2-SVP[28] (def2-ecp for "Ru")[29] basis set by employing Turbo mole 6.4 suite of programs.[30] The resolution of Identity (ri)[31] and multipole accelerated resolution of Identity (marij)[32] approximations with dispersion correction (disp3)[33] have been used for all the calculations. Solvent corrections were incorporated in all calculations using the COSMO model,[34] with methanol ($\varepsilon = 32.7$) as the solvent. Mercury 4.0.0[35] software was used for visualization.

Time-dependent density functional theory (TD-DFT)[36] calculations were carried out by employing the Gaussian 09 program[37] with CAM-B3LYP/def2SVP level of theory.[38] An implicit conductor-like polarizable continuum solvation model (CPCM)[39] was used to consider the solvent effect of methanol. Previously obtained optimized geometries for **C2** and **C6** were taken as input for the calculations, and the data for the corresponding UV–Vis spectra were obtained.

2.6 | DNA binding experiments

2.6.1 | Binding study using absorption spectroscopy

UV spectroscopy was employed to study the interaction of compounds with CT DNA and to investigate the possible binding modes of CT DNA. Absorption titrations were carried out with constant compound concentrations while changing the CT-DNA concentration within. Stock solution of the complexes was diluted with tris buffer to get the desired concentration (30 μM). Equal increments of CT-DNA were added at different ratios to the compound solution and the reference solution to eliminate the absorbance of CT-DNA itself, while measuring the absorption.

2.6.2 | DNA-EB competitive binding studies

The competitive binding and the mode of binding with DNA have been investigated with fluorescence spectroscopy in order to examine whether the complexes can displace EB from the DNA–EB complex and bind to DNA through intercalation. The DNA–EB complex was prepared by adding EB and DNA in tris buffer. A certain amount of a solution of each complex was added step by step into the solution of the DNA–EB complex. The influence of the addition of each complex has been obtained by recording the variation in the fluorescence emission spectra of the DNA–EB complex. The fluorescence intensities were measured at 609 nm (524 nm excitation) after addition of different concentrations of the complexes at different ratios.

2.6.3 | Viscosity measurement

The relative viscosity of DNA (200 μM) solutions was measured by Cannon–Ubbelohde viscometer at a constant temperature of 32.0 ± 0.1°C in the presence of complexes **C1–C8.** The [complex]/[DNA] ratios were fixed at 0, 0.04, 0.08, 0.12, 0.16, and 0.20 in Tris–HCl buffer (pH 7.2). Digital stopwatch with least count of 0.01 s was used for flow time measurement with accuracy of ±0.1 s. The flow time of each sample was measured three times, and an average flow time was calculated. The data are plotted as $(\eta/\eta_0)^{1/3}$ versus [complex]/[DNA], where η_0 and η is the viscosity of the DNA solution in the absence and presence of complex, respectively. Viscosity values were calculated from the observed flow time of DNA-containing solutions (t) corrected for that of the buffer alone (t_0), $\eta = (t - t_0)/t_0$.[40]

2.7 | BSA binding experiments

The BSA-binding study was performed employing steady state fluorescence spectroscopy. A solution of bovine serum albumin (BSA, 16.6 μM) in buffer (containing 15-mM tri-sodium citrate and 150-mM NaCl at pH 7.0) was used to carry out the tryptophan fluorescence quenching experiments. The quenching of emission intensity of the tryptophan residues of BSA at 343 nm was monitored in the presence of increasing concentrations of the complexes.[41] Fluorescence spectra were recorded from 300 to 500 nm at an excitation wavelength of 296 nm.

2.8 | Evaluation of anticancer activity

The synthesized complexes were assessed for their cytotoxic activity by standard MTT colorimetric assay.[42] HeLa cells (5.0×10^3 cells well^{-1}) were placed in 96-well culture plates (Tarson India Pvt. Ltd.) and grown overnight at 37°C in a 5% CO_2 incubator. **C1–C8** were added to the wells in the concentration range 0.5–150 mg/ml; control wells were prepared by addition of culture medium without the compounds. The plates were incubated at 37°C in a 5% CO_2 incubator for 48 h and standard 3-(4,5-dimethylthiazole)-2,5-diphenyltetraazolium bromide MTT dye solution was added to each well. After 4 h of incubation, the culture media was thrown out, and the wells were washed with phosphate buffer saline (Hi-Media, India Pvt. Ltd.), which was followed by addition of DMSO to dissolve the formazan crystals formed and further incubation for 30 min. The optical density of each well was measured spectrophotometrically at 563 nm using Biotek-ELX800MS universal ELISA reader (Bio-Tek instruments, Inc., Winooski, VT). The IC_{50} values were determined by plotting the percentage viability versus concentration on a logarithmic graph and reading off the concentration at which 50% of cells remained viable relative to the control. Each experiment was repeated at least three times to obtain mean values.

3 | RESULTS AND DISCUSSION

3.1 | Synthesis of the $[(Ru(\eta^6\text{-}p\text{-}cym)_2L)_2(\mu\text{-}im/azpy)]Cl_{1-2}$ complexes

A new series of binuclear ruthenium (II) arene complexes of the type $[(Ru(\eta^6\text{-}p\text{-cym})L)_2(\mu\text{-im/azpy})]Cl_{1-2}$ (**C1–C8**) were achieved by reacting the mononuclear complexes $[Ru(\eta^6\text{-}p\text{-cym})(L)Cl]$ with the bridging ligand imidazole/4,4′-azopyridine in the ratio 2:1, in CH_2Cl/CH_3OH mixture, as shown in Figure 2. The synthesized complexes were found to be stable in air at room temperature and non-hygroscopic. The elemental analysis data for the complexes matched well with the calculated values, thus confirming their proposed composition.

3.2 | Characterization

The ESI-mass spectra (Figure S1) show m/z peaks corresponding to the molecular ions that give evidence of the formation of binuclear complexes with the bridging ligand. Due to the large size of the complexes, various fragments may be formed during ionization. Fragmentation of the complexes by removal of the bridging and/or the terminal ligand(s) can occur. Fragmentation of the ligand backbone while the ligand is still bound to the metal ion often occurs. The formation of the peaks (Table S1) with their assigned m/z values may be rationalized in the following way. Loss of a hydrogen atom H from the organic ligand framework tends to yield a (M − 1) peak whereas the (M + 1) peak is due to protonated molecular ion $(M + H)^+$. The molecular ion peak values for the complexes indicate that a *p*-cymene and a bidentate pyrazole-thiosemicarbazone ligand is coordinated to each of the two Ru(II) ions with an imidazole or a 4,4′-azopyridine ligand bound simultaneously to both the metal centers. Thus, each of the Ru(II) ions is six coordinated with a distorted octahedral geometry. The complexes **C1–C4** and **C5–C8** have molar conductance (10^{-3} M in DMSO) in the range of 72–75 (Ω^{-1} m^2 M^{-1}) and 131–135 (Ω^{-1} m^2 M^{-1}), respectively, at 38°C suggesting 1:1 and 1:2 electrolytic behavior.[43]

In the IR spectra of the complexes **C1**–**C8**, the free ligand $\nu_{(C=S)}$ asymmetric and symmetric absorption in the region 1260–1290 and 807–824 cm^{-1} is shifted to a single $\nu_{(C-S)}$ absorption at 748–775 cm^{-1}, due to enolization of –NH–C=S and subsequent co-ordination via deprotonated sulfur. The strong band in the range 1597–1599 cm^{-1} characteristic of the azomethine group ν(C=N) is shifted to 1590–1588 cm^{-1}[[17]] due to coordination through the azomethine nitrogen atom. The bands in the fingerprint regions 2959–2970 cm^{-1} and 1457–1638 cm^{-1} owing to aromatic ν_{C-H} stretch and aromatic $\nu_{C=C}$ in plane vibrations, respectively, are indicative of presence of *p*-cymene in all the complexes. Characteristic band around 3300–3364 cm^{-1} due to the $\nu_{(N-H)}$ stretching of the free imidazole was found to be absent in the spectra of C1–C4, while the $\nu_{N=N}$ stretching of the 4,4′-azopyridine ligand is observed at 1402–1487 cm^{-1} in the spectra of **C5**–**C8**. The analysis of the IR spectra suggests that all the pyrozlyl thiosemicarbazones act as monoanionic bidentate ligands and interact with the metal center via the azomethine group and deprotonated sulfur. The IR spectra of all the complexes have been provided as supporting information (Figure S2).

The ^{1}H NMR spectra of **C1**–**C8** (Figure S3) show distinct peaks corresponding to *p*-cymene. The presence of a *p*-cymene ligand was confirmed by the presence of 6-proton doublet at $\delta = 1.93$–1.02 ppm owing to two methyl protons of *iso*-propyl group [CH$(CH_3)_2$], 3-proton singlet at $\delta = 2.49$–1.91 ppm due to the Ar-methyl group *para* to the *iso*-propyl group, 1-proton quartet at $\delta = 3.95$–2.24 ppm attributed to –CH of the *iso*-propyl group, and two 2-proton doublets at $\delta = 7.01$–5.44 ppm assigned to the 4 Ar-protons of *p*-cymene.[44] The imine proton observed in the range $\delta = 8.36$–10.17 ppm in free ligands is shifted upfield at $\delta = 8.22$–8.69 ppm in the complexes indicating coordination via HC=N. All the aromatic protons present in pyrozole ring are observed in the excepted region. The absence of a singlet at $\delta = 11$–13 ppm owing to the N–H proton of free imidazole,[34] in the NMR spectra of **C1**–**C4**, suggests co-ordination of the deprotonated imidazole N with the metal center. Apart from this, CH=CH proton of imidazole at $\delta = 7.75$–7.93 ppm is observed in spectra of **C1**–**C4** indicating the presence of imidazole ring. In case of **C5**–**C8**, a slight upfield shift of the doublet peak due to four protons in the pyridine ring of 4,4′-azopyridine is observed at $\delta = 7.28$–8.48 ppm compared with ^{1}H NMR of pure 4,4′- azopyridine at $\delta = 7.75$–8.89 ppm, indicating its co-ordination to the metal center(s).[45]

The electronic absorption spectra of the complexes **C1**–**C8** (Figure S4) show two major bands in the wavelength range 200–700 nm. The red shift of the intense absorption bands at 223–227 nm assigned to intra-ligand $\pi \rightarrow \pi^*$ transition of the ligand aromatic rings to 226–230 nm in the complexes is attributed to their coordination with Ru(II) metal center. Another medium intensity peak owing to the intraligand N and S centered $n \rightarrow \pi^*$ transitions, in the range of 358–380 nm have blue shifted to 313–365 nm on complexation. This shift in the wavelength indicates N and S coordination of the thiosemicarbazone ligand to the metal center. For complexes **C5**–**C8**, one additional peak was observed within 264–278 nm, due to the intraligand $n \rightarrow \pi^*$ transitions of the azopyridine moiety.[46] The λ_{max} values of all the transitions taking place in the complexes have been tabulated in Table S2.

Full geometry optimizations of compounds were carried out using the DFT method at b-p functional and def2-SVP (def2-ecp for "Ru") basis set by employing Turbomole 6.4 suite of programs as mention above in Section 2.5. This functional has been shown to give more accurate results for organometallic complexes. All calculations were performed using the approximations with dispersion correction (disp3) program. The DFT calculations for geometry optimization provide some insight into the structure of the complexes. Optimized structures of the complexes **C1** and **C5** are shown in Figure 1. Pianostool type geometry is seen around each metal center of the binuclear complexes with the Ru(II) ions π-bonded to the arene ring. The average Ru–Ru distance in the binuclear complexes with imidazole as bridging ligands is 6.14 Å, whereas in complexes with 4,4′–azopyridine as bridging ligands, the average distance is 13.26 Å due to the presence of longer 4,4′-azopyridine ligand. The bond angle values reveal a pseudo octahedral coordination of the ruthenium centers. The metal–ligand bond lengths and bond angles tabulated in Table 1 are in well agreement with the values in the literature.[47,48] Optimized structures of the rest of the complexes are given in Figure S5.

In the absence of XRD data, time-dependent density functional theory (TD-DFT) calculations were done to provide further evidence for the bridging structure by correlating the experimentally observed UV–Vis spectra with the corresponding computationally obtained data. Two complexes **C2** and **C6**, one each from the imidazole and azopyridine bridged series, were selected for the calculations. The previously obtained optimized structures were used as input geometries for the TD-DFT calculations, and the UV–Vis spectral data generated (Table S3) was found to be in close agreement with the experimentally observed UV–Vis spectra.

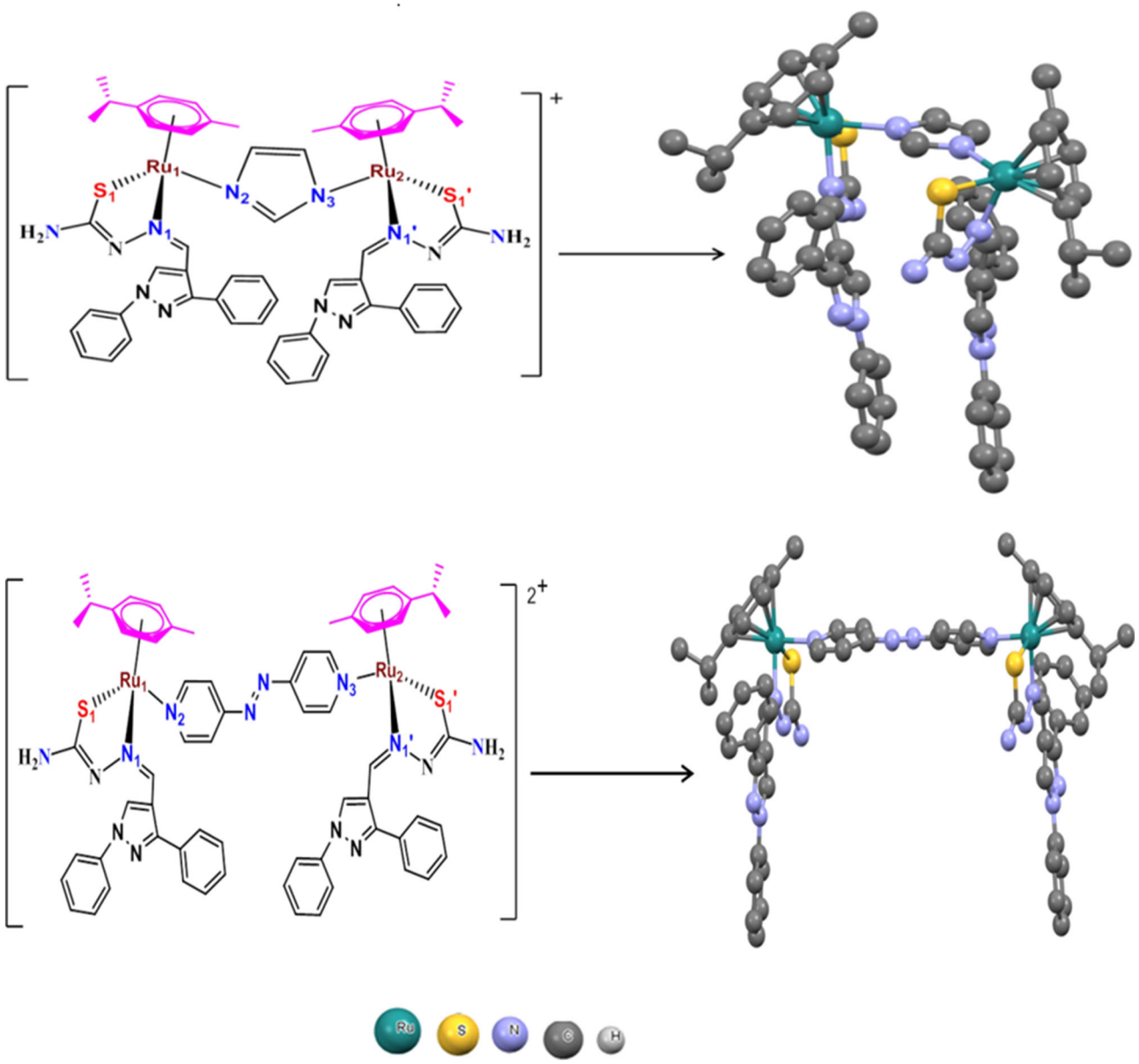

FIGURE 1 Optimized structures of the complexes **C1** and **C5**

3.3 | Stability studies

Due to the less aqueous solubility of the metal complexes, DNA/BSA binding and cytotoxicity studies were carried out using stock solutions of the complexes prepared in DMSO. The solutions were then diluted with tris buffer so that the test solutions contained no more than 2% DMSO. To check the stability of the complexes in DMSO, UV–Visible spectra of the complexes **C1**–**C8** were recorded at room temperature in the range 200–700 nm at time intervals up to 48 h. No changes in the UV–Vis spectra were observed, implying that the complexes are stable in DMSO solution.

3.4 | DNA binding studies

One of the primary targets for many metallotherapeutics (e.g., cisplatin, carboplatin, and oxaliplatin) and organic anticancer drugs (doxorubicin, gemcitabine, 5-fluorouracil, etc.) is the nucleus DNA of the cancer cells.[49] Significant emphases have been given to the design of complexes with ligand scaffolds that bind to DNA with site selectivity. Several Ru(II) complexes have shown significant DNA binding affinity.[50] The binding mode and affinity between complexes under study and CT-DNA were evaluated by the viscosity measurements, UV–Vis absorption, and fluorescence emission spectroscopy.

	L1		L2		L3		L4	
Bond Length (in Å)	**C1**	**C5**	**C2**	**C6**	**C3**	**C7**	**C4**	**C8**
Ru1 ... ... Ru2	6.15	13.29	6.17	13.26	6.13	13.26	6.11	13.26
Ru1–N1	2.09	2.10	2.09	2.09	2.09	2.09	2.09	2.09
Ru1–S1	2.36	2.36	2.37	2.36	2.36	2.36	2.36	2.37
Ru1–N2	2.09	2.10	2.09	2.10	2.09	2.10	2.08	2.09
Ru2–N1′	2.09	2.10	2.08	2.09	2.08	2.09	2.08	2.09
Ru2–S1′	2.39	2.36	2.42	2.36	2.40	2.36	2.40	2.37
Ru2–N3	2.09	2.10	2.10	2.10	2.10	2.10	2.10	2.09
Bond angle (in degree)								
S1–Ru1–N1	80.9	81.1	80.7	81.2	81.0	81.1	81.1	81.0
S1–Ru1–N2	89.3	90.1	90.2	89.2	88.2	89.0	88.4	88.7
N1–Ru1–N2	81.2	84.6	84.2	84.3	83.0	84.6	83.4	84.4
S1′–Ru2–N1′	79.0	81.0	78.2	81.1	78.8	81.2	78.8	81.0
S1′–Ru2–N3	93.5	90.1	93.8	89.2	93.3	89.2	93.4	88.5
N1′–Ru2–N3	83.4	84.6	83.4	84.3	83.2	84.7	82.7	84.3

TABLE 1 Metal ligand bond lengths and bond angles of complexes under study obtained from geometry optimization

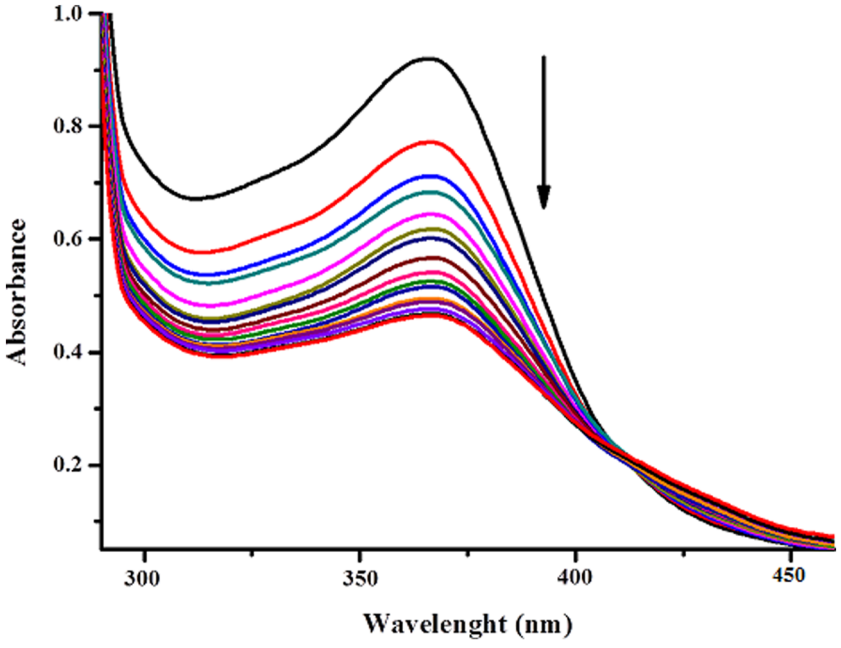

FIGURE 2 UV absorption spectra of **C1** at increasing concentrations of CT-DNA, the arrow shows decrease in intensity upon increasing concentration of the complex

3.4.1 | Binding study using absorption spectroscopy

Absorption titration method was employed to evaluate the binding ability of the complexes to CT-DNA. The UV spectra of all the complexes (10^{-6} M) have been recorded in the absence and presence of varying CT-DNA concentration (at [DNA]/[**C**] ratio of 0–3.01) (Figure 2). **C1–C8** showed hypochromism (50.5%–58.6%) accompanied with a blue shift (1–3 nm) indicating an intercalative interaction with DNA. The titration plots of remaining complexes have been provided in Figure S6. The binding constants $\boldsymbol{K_b}$, for the complexes were calculated from the Mehan's equation.[51]

$$[\mathrm{DNA}]/(\varepsilon_\mathrm{A}-\varepsilon_\mathrm{f}) = [\mathrm{DNA}]/(\varepsilon_\mathrm{b}-\varepsilon_\mathrm{f}) + 1/\mathrm{K_b}\,(\varepsilon_\mathrm{b}-\varepsilon_\mathrm{f}),$$

where [DNA] is the concentration of DNA in base pairs, $\varepsilon_\mathrm{A} = \mathrm{A_{obsd}}/[\mathrm{compound}]$, ε_f is the extinction coefficient for the unbound compound, and ε_b is the extinction coefficient for the compound in the fully bound form. The plot of $[\mathrm{DNA}]/(\varepsilon_\mathrm{A}-\varepsilon_\mathrm{f})$ versus [DNA] (Figure S7) gave a slope $1/(\varepsilon_\mathrm{b}-\varepsilon_\mathrm{f})$ and an intercept $(1/\mathrm{K_b})(\varepsilon_\mathrm{A}-\varepsilon_\mathrm{f})$. $\mathbf{K_b}$, the intrinsic binding constant, is the ratio of the slope to the

intercept. The binding constants values, calculated for **C1**–**C8** (Table 2) in the range of 1.6×10^4–1.2×10^5 M^{-1} reveal strong binding of the complexes with the biomolecule. Slightly higher K_b values in the range of $(1.60–2.17) \times 10^5$ M^{-1} were obtained for half-sandwich Ru(η^6-*p*-cymene) complexes with the pyrazole-based ligands [2-(1*H*-pyrazol-3-yl)pyridine (**L1**), 3-(furan-2-yl)-1*H*-pyrazole (**L2**), and 3-(thiophen-2-yl)-1*H*-pyrazole (L3)][52] and 2.47×10^5 and 3.73×10^5 M^{-1}, respectively, for the mononuclear and binuclear Ru(η^6-*p*-cymene) complexes containing the indole thiosemicarbazone ligand.[53] However, the binding constant values are comparable with those observed in the case of Ni(II) bis (thiosemicarbazone) complexes ($1.40–2.90 \times 10^{-4}$ M^{-1}) and binuclear Ni(II) complexes ($1.17–11.6 \times 10^4$ M^{-1}).[54] The effect of size, shape, hydrophobicity, and electrolytic behavior of the metal complexes play significant roles in binding of the complexes to DNA.[55] It is observed that the complexes **C3**, **C7**, **C4**, and **C8** with 4-phenyl/napthyl substituted thiosemicarbazone ligand show high binding affinities due to the additional planar aromatic rings present in their ligand scaffolds which facilitate hydrophobic interactions with the nucleobases.[56] **C1**, **C5**, **C2**, and **C6** with 4-hydrogen/methyl substituted thiosemicarbazone ligand display low binding affinities due to no additional planar aromatic rings. The standard Gibb's free energy for DNA binding was calculated using the following relation.[57]

$$\Delta G^{\circ}_{b} = -RT \ln K_b,$$

where R is universal gas constant and T is temperature. All the complexes are showing negative value of ΔG°_{b} indicating spontaneity of reaction.

3.4.2 | EB displacement study using emission spectroscopy

EB displacement experiment was carried out to confirm the intercalative mode of binding of the complexes as suggested by absorption titration study. The emission spectra of the DNA-EB adduct ($\lambda_{ex} = 546$ nm, $\lambda_{em} = 610$) in the absence and presence of increasing amounts of complexes (at a [C]/[DNA–EB] ratio of 0–0.62) have been recorded. Addition of complexes resulted in decrease in the intensity of the emission band at 610 nm up to 35.02%–42.67% indicating that the complexes compete with EB in binding to DNA (Figure 3). The observed quenching of DNA–EB fluorescence on addition of the complexes suggests that they intercalate DNA by displacing EB from the DNA–EB complex. The titration plots of remaining complexes have been shown in Figure S8.

The quenching constant (K_{SV}) values were calculated from the slopes of straight lines obtained from the Stern-Volmer equation[58]:

$$Io/I = 1 + K_{SV}[Q],$$

where Io and I are the emission intensities in the absence and the presence of the quencher **C1-C8** respectively, [Q] is the concentration of the quencher, and K_{SV} is the Stern-Volmer constant which can be obtained from the slope of the plot of Io/I versus [Q] (Figure S9). The plots illustrate that the quenching of DNA–EB fluorescence by the complexes is in good agreement (R = 0.98) with the linear Stern-Volmer equation. The Stern-Volmer quenching constant K_{SV} values with standard deviations (SD) given in Table 2 are in the range of $(1.1–9.2) \times 10^4$ M^{-1}.

3.4.3 | DNA viscosity measurement

To further confirm the proposed intercalative mode of interaction between the complexes and DNA, viscosity measurements were carried out in the absence and in the presence of the complexes added gradually. A steady increase in the relative viscosity of CT-DNA was observed on increasing the concentrations of the complexes (0–200 μM) in Tris–HCl/NaCl buffer (200 μM). The

TABLE 2 K_b and K_{SV} values of complexes

Code	K_b M^{-1}	K_{SV} M^{-1}	λ shift	ΔG° kJmol^{-1}
C1	$2.8 \times 10^4 \pm 0.007$	$1.1 \times 10^4 \pm 0.035$	2 nm	−25.37
C2	$4.6 \times 10^4 \pm 0.009$	$5.5 \times 10^4 \pm 0.027$	1 nm	−26.60
C3	$7.2 \times 10^4 \pm 0.017$	$1.7 \times 10^4 \pm 0.036$	1 nm	−27.71
C4	$6.8 \times 10^4 \pm 0.041$	$1.3 \times 10^4 \pm 0.042$	1 nm	−27.57
C5	$2.6 \times 10^4 \pm 0.026$	$9.2 \times 10^4 \pm 0.036$	2 nm	−25.19
C6	$1.6 \times 10^4 \pm 0.012$	$3.1 \times 10^4 \pm 0.028$	3 nm	−23.98
C7	$\mathbf{1.1 \times 10^5 \pm 0.032}$	$6.0 \times 10^4 \pm 0.036$	2 nm	−28.76
C8	$\mathbf{1.2 \times 10^5 \pm 0.120}$	$4.3 \times 10^4 \pm 0.042$	1 nm	−28.98

relative viscosity slopes of the DNA solutions in the presence of the complexes were calculated (slope values 0.44–0.49) and compared with the classical intercalator ethidium bromide (slope value of 0.94). Thus the insertion of complexes in between the base pairs elongates the double helix, leading to an increase in the viscosity of DNA. Complexes binding with DNA grooves cause less noticeable or no variation in the viscosity.[52] The effects of **C1**–**C8** on the viscosity of CT-DNA solution are shown in Figure 4. With increasing [complex]/[DNA] concentration ratios, the relative viscosity of CT-DNA increased gradually speculative of intercalative mode of binding.[54]

3.5 | BSA binding studies

Literature have revealed that there can be electrostatic, hydrophobic and van der Waals interactions between BSA and metal complexes and also and hydrogen bond formation. Fluorescence spectrophotometry is a common technique to study molecular interaction with BSA. The fluorescence emissions of the serum protein are due to tyrosine, tryptophan, and phenylalanine residues. The effect of addition of the complexes on the fluorescence emission of BSA was monitored to evaluate the interaction of the complexes with the protein. Addition of

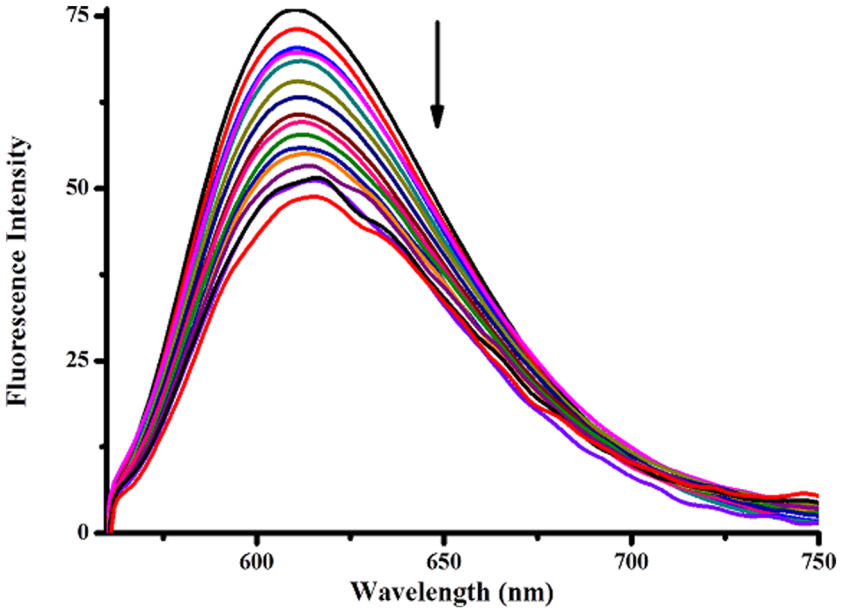

FIGURE 3 Plot of fluorescence emission intensity I versus wavelength λ for CT DNA-EB complex at different concentrations of **C1**, the arrow shows decrease in fluorescence intensity on increasing concentration of the complex

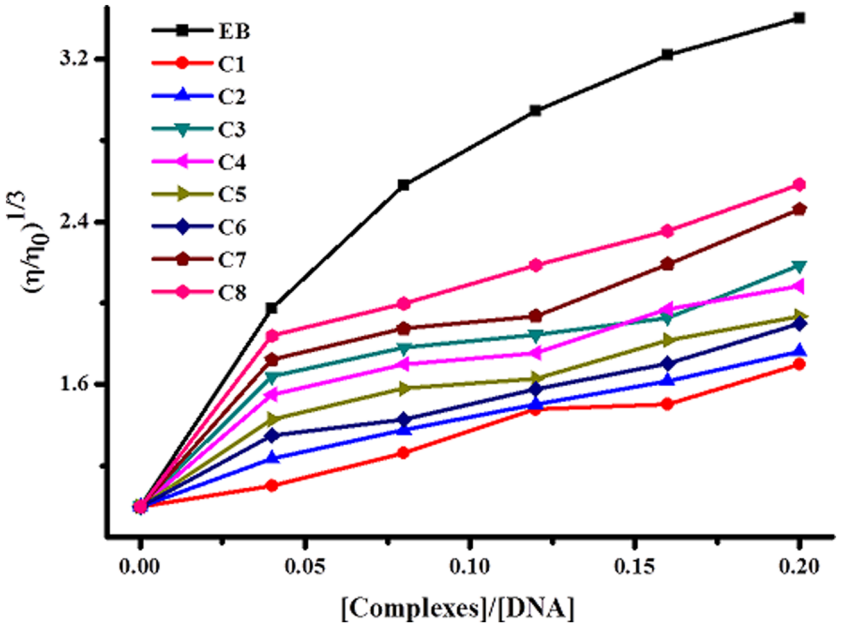

FIGURE 4 Effect of increasing amounts of the complexes and ethidium bromide on the relative viscosity of CT-DNA (200 mM) in Tris–HCl buffer at 32°C. [Complex]/[DNA] = 0, 0.04, 0.08, 0.12, 0.16 and 0.20

increasing concentrations of the complexes to a solution of BSA (at [C]/[BSA] ratio of 0–2.8) results in a significant decrease of the protein fluorescence intensity at 344 nm (Figure 5). The observed hypochromism with a small blue shift (~2 nm) in the presence of **C1–C8** indicates a static quenching of BSA fluorescence by the complexes.[59] The complexes interact hydrophobically with proteins, which is evident from the observed hypochromism. The titration plots of remaining complexes are shown in Figure S10. The values of the Stern-Volmer quenching constant (K_{SV}) obtained from the plot of [Io/I] versus [Q] (Figure S11), for the complexes interacting with BSA are in the order of 10^4–10^5 M^{-1} (Table 3). This indicates strong interaction with the protein. The K_{SV} values reveal that the complexes are more efficient in quenching the fluorescence of BSA compared with the ligands (10^3–10^4 M^{-1}) due to increased hydrophobicity. The plot of log [(Io − I)/I] versus log [Q] for all the complexes (Figure S12) is linear; the association binding constant (K_a M^{-1}), and the number of binding sites per albumin (n) have been obtained by double logarithm equation.[60] The Ka values for the complexes are within the range of 10^5–10^6 M^{-1} as expected from a good BSA carrier activity in vivo.[61]

$$\log (\mathrm{Io} - \mathrm{I})/\mathrm{I} = \log \mathrm{K_a} + \mathrm{n} \log [\mathrm{Q}]$$

The K_a values in the order of 10^5–10^6 M^{-1} also indicate strong binding of the complexes to BSA in agreement to the K_{sv} values. The linear nature of the double logarithm plots and the n values calculated for **C1-C8**, indicate that only one of the tryptophan residues on BSA protein is interacting with the complexes.

3.6 | Docking studies

Molecular docking study was employed to identify the principle binding site of both the complexes with DNA and the BSA protein. Crystal structure of DNA and BSA were obtained from the Brookhaven Protein Database (PDB) (http://www.rcsb.org/pdb). Structures of the complexes **C3** and **C7** were created in ACD/Chemsketch 12.01 software[62] (Figure S13) and converted into .mol file format to .pdb by Argus Lab. Molecular docking of the selected complexes with DNA (PDB: 1BNA) and BSA (PDB ID: 4F5S) were analyzed and visualized using Argus Lab 4.0.1.[63] Argus Lab is a docking tool based on Lamarckian genetic algorithm having exact grid resolution along with precise predictions of the ligand binding sites.

"AScore" scoring function was selected for the docking studies. The docking algorithm was set as Argus dock with exhaustive search and the grid resolution was fixed to

TABLE 3 K_{SV}, K_a, and n values for complexes

Code	K_a M^{-1}	K_{SV} M^{-1}	n
C1	$1.5 \times 10^5 \pm 0.187$	$1.4 \times 10^5 \pm 0.235$	1.0
C2	$1.1 \times 10^6 \pm 0.191$	$9.9 \times 10^4 \pm 0.173$	1.2
C3	$7.1 \times 10^5 \pm 0.186$	$1.5 \times 10^5 \pm 0.208$	1.1
C4	$1.6 \times 10^6 \pm 0.184$	$1.6 \times 10^5 \pm 0.164$	1.2
C5	$3.6 \times 10^5 \pm 0.185$	$8.1 \times 10^5 \pm 0.154$	1.3
C6	$1.6 \times 10^5 \pm 0.185$	$1.0 \times 10^4 \pm 0.148$	1.4
C7	$1.2 \times 10^6 \pm 0.183$	$8.1 \times 10^5 \pm 0.180$	1.2
C8	$4.3 \times 10^6 \pm 0.187$	$5.6 \times 10^5 \pm 0.152$	1.3

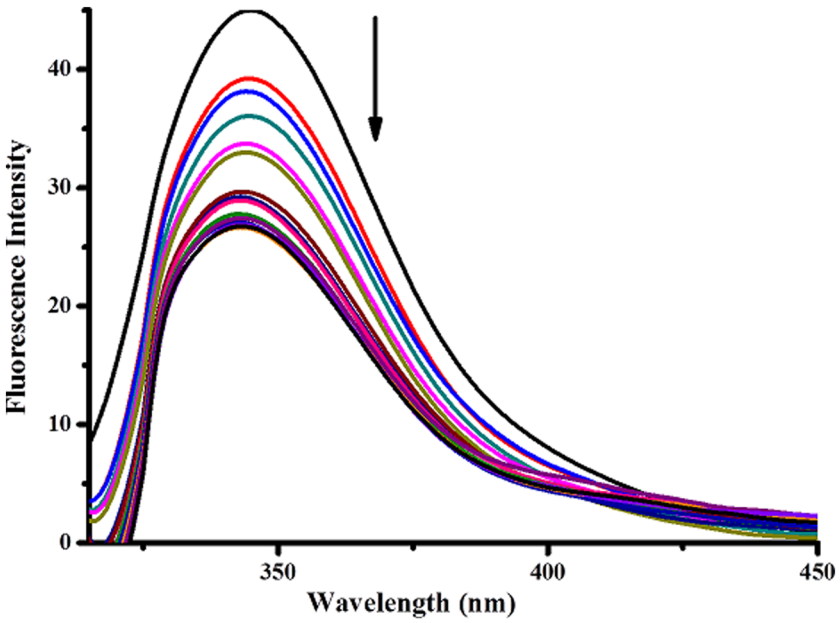

FIGURE 5 Plot of Fluorescence emission intensity versus wavelength for BSA at increasing concentrations of **C1**, the arrow shows decrease in the fluorescence intensity with increasing concentration of the complex

4 Å. The size for binding box was set to 22.48 Å × 26.74 Å × 43.40 Å for **C3** and 22.48 Å × 26.16 Å × 42.48 Å for **C7** with DNA, and 17.08 Å × 27.99 Å × 15.50 Å for **C3** with BSA, respectively. The ligand docking method used for following studies was set to "Flexible mode" and the precision factor was set to "Regular."

The stability of docked poses was decided by ArgusLab energy functions and the hydrogen bonds formed between receptor and ligands.[64] Further 3D, figure for BSA-**C3** interactions, was also generated by "Protein-Ligand Interaction Profiler." The tool gave us the idea regarding hydrophobic interaction and π-stacking interaction.[65]

Validation of the docking interactions for the selected complexes **C3** and **C7** with DNA (PDB: 1BNA) are shown in Figures S14–S16. It was observed that both the complexes showed complete base stacking interaction with DNA, where the nitrogen base sequence in one strand is $C_1G_2C_3G_4A_5A_6T_7T_8C_9G_{10}C_{11}G_{12}$ and for the complementary sequence is $G_{24}C_{23}G_{22}C_{21}T_{20}T_{19}A_{18}A_{17}G_{16}C_{15}G_{14}C_{13}$. The most significant binding interaction was based on the hydrogen bond formed between complex-DNA interfaced to the substrate binding site. The hydrogen bond less than 3 Å was considered. **C3** was found to be interacting with thymine nitrogen base at positions 7 and 8 (Table S4) whereas **C7** was found to be interacting both with adenine at position 6 and 18 and thymine at positions 7, 8, and 19 (Table S5).

Preferable binding site of **C3** with BSA is given in Table S6. In order to explain the interaction, hydrogen bond less than 4 Å was considered. **C3** showed significant hydrogen bond interaction with Ser219, Tyr331, Trp213, and Arg217 of chain A. Protein–Ligand Interaction Profiler tool postulated the hydrophobic and π-stacking interactions explaining the hydrophobic interaction playing a major role in the binding of the ruthenium complex with BSA (Figure S17; Tables S7 and S8). The amino acid found to involve in hydrophobic interactions were Ala212, 216, 225; Trp213; Val215, 230, 292, 342; Leu218, 330, 346; Lys221; Phe222, 227; Glu226; Tyr331.

Drugs usually bind to BSA at two major sites Sudlow's site 1 and site II having specialized cavity of subdomain IIA and IIIA.[66] The important ligand binding site on BSA is located in the subdomains IIA and IIIA, which are the Sudlow sites.[67] Above interactions suggest that **C3** binds to BSA in the hydrophobic cavity of Site I in subdomain IIA.[68] **C3** is capable of quenching the tryptophan fluorescence by binding to the hydrophobic region of protein facilitated by hydrophobic interaction of methyl and isopropyl groups of *p*-cymene and the aromatic groups of the pyrazolyl thiosemicarbazone ligand. Thus the ligand hydrophobicity contributes to the BSA protein binding affinity of the complex.

3.7 | In silico ADME toxicity profile

ADME explains the absorption, distribution, metabolism and excretion of the ligands designed, particularly drugs. SwissADME (http://www.swissadme.ch/) is one of the online tools which elucidate the pharmacological and toxicological properties of a drug/complex. In the present study, the simplified molecular input line entry specifications (SMILES) were uploaded into the database. This leads to the generation of result in the form of Boiled egg.[69] The tool gives all the data related to physicochemical properties, lipophilicity, water solubility, pharmacokinetics, druglikeness, and medicinal chemistry.[70]

ADME properties of the complexes **C3** and **C7** were evaluated. The results (Table S9) reveal that the ruthenium complexes were showing low gastrointestinal (GI) absorption along with no blood brain barrier permeation. Even though they showed interaction with P-gp substrate but no inhibitory action was observed with cytochrome P450 enzymes. This explains that the drugs can be properly metabolized and can be eliminated from the system without damaging cytochrome P450 enzymes.

3.8 | Antiproliferative studies

Since the DNA and BSA binding studies indicated a reasonably strong interaction of the complexes with the biomolecules, MTT assay was carried out in a dose dependent fashion to analyze the antiproliferative activity of the binuclear complexes **C1**–**C8** with HeLa (human cervical cancer) for an incubation period of 48 h. This cell line was selected due to higher occurrence of cervical cancer in human population worldwide, which is of prime concern. After the incubation period, the % of viable cancer cells was reduced. The plot of percentage of cell viability versus complex concentration (Figure 6) depicted the dose dependent cell death induced by the tested compounds. The corresponding IC_{50} values are given in Table 4. The IC_{50} values of the synthesized ruthenium complexes in the range of 17.3–41.3 μM reveal that they show moderate cytotoxicity in HeLa cells and are less active compared with *cis*-platin ($IC_{50} = 18.8 \pm 3.4$ μM) except **C2** ($IC_{50} = 17.3 \pm 1.82$ μM). The anticancer activities are in the order of **C2** > **C8** > **C1** > **C3** > **C4** > **C5** > **C6** > **C7**. **C2** with a IC_{50} value lower than that of cisplatin shows the highest cytotoxicity followed by **C8** ($IC_{50} = 23.7 \pm 8.90$ μM). The high DNA binding affinity and enhanced cytoxicity indicate DNA to be the target molecule for **C8.** However, the order of cytotoxicity of the complexes **C1**–**C7** is not in line with their DNA binding capabilities which suggest that DNA may not be the target for the complexes

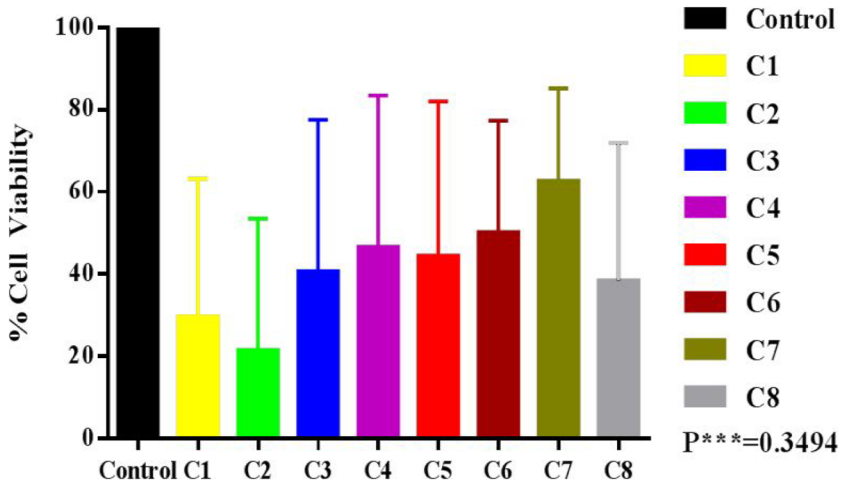

FIGURE 6 Percent cell viability verses concentration plots of **C1**–**C8** on HeLa Human cervical cancer cell lines. Each point is the mean ± standard error obtained from three independent experiments

TABLE 4 The IC_{50} values for the human cervical cancer cell line HeLa with **C1**–**C8** for 48 h

Code	**C1**	**C2**	**C3**	**C4**
μM	24.4 ± 2.96	17.3 ± 1.82	29.6 ± 5.14	31.7 ± 3.24
Code	**C5**	**C6**	**C7**	**C8**
μM	32.6 ± 2.04	35.9 ± 5.71	41.3 ± 11.44	23.7 ± 8.90

in vitro. Also, high positive charge (+2) on **C8** may result in electrostatic interactions between the positively charged $[(Ru(p\text{-cym})L)_2(\mu\text{-azpy})]^{2+}$ complex and the negatively charged polar head groups of the lipid bilayer of the cell membrane, hence an enhanced cellular uptake. In contrast, the complexes **C5**–**C7** with +2 charges exhibit lower antitumor activity, which suggests that enhanced cellular uptake may not always lead to enhanced cytotoxicity. The complexes were found to be more active against HeLa cells compared to Ru(II)-arene complexes with triarylamine-thiosemicarbazone hybrid ligands except for one complex as reported.[20]

4 | CONCLUSION

Binuclear Ru(II) complexes of *p*-cymene and the pyrazol-thiosemicarbazone hybrid ligands were synthesized and characterized using various spectral techniques. The complexes showed good binding propensities towards DNA ($K_b = 10^4$–10^5 M^{-1}) and BSA ($Ka = 10^5$–10^6 M^{-1}) as revealed by their binding studies. The binuclear complexes were found to have better binding affinities towards DNA/BSA due to their enhanced hydrophobicity compared to their mononuclear analogues. DNA docking studies of **C3** and **C7** revealed base stacking interactions and formation of H-bonds with thyamine and adenine bases. In addition BSA docking studies of complex **C3** indicated H- bond formation with the amino acid residues Ser219, Tyr331, Arg217, and Trp213. Hydrophobic and stacking interactions with the protein were also observed. **C1**-**C8** were found to be more active than some of the Ru(II)-arene complexes with hybrid TSC ligands. The complex **C2** showed more cytotoxicity compared to *cis* platin towards HeLa cancer cells.

ACKNOWLEDGMENTS

P.K. greatly acknowledge the University Grants Commission, New Delhi, for the financial assistance, MRP fellowship (UGC F.No. 43-238/2014(SR)), RFSMS-BSR fellowship (Letter no. F.5-71/2007(BSR)), and DST-PURSE fellowship (Letter no. FS/206/19-20), respectively. The author would like to acknowledge the DST-FIST program for funding NMR facility at the Department of Chemistry, Faculty of Science, and The Maharaja Sayajirao University of Baroda. The author is thankful to the Heads, Department of Chemistry and Zoology, Faculty of Science, The Maharaja Sayajirao University of Baroda, for providing the necessary laboratory and instrumentation facilities to carry out the research work. The author is thankful to the Centre of Excellence in Scientific Computing (COESC), CSIR-NCL Pune, for providing computational facilities.

AUTHOR CONTRIBUTIONS

Priyanka Khanvilkar: Formal analysis; methodology; software. **Soumya Dash:** Software. **Devjani Banerjee:** Software. **Aliasgar Vohra:** Formal analysis. **Ranjitsinh**

Devkar: Formal analysis; resources; supervision. **Debjani Chakraborty:** Investigation; supervision.

CONFLICT OF INTEREST

The authors declare that there is no conflict of interest regarding the publication of this article.

DATA AVAILABILITY STATEMENT

The data that supports the findings of this study are available in the supporting information of this article.

ORCID

Priyanka Khanvilkar https://orcid.org/0000-0001-5938-9725
Soumya R. Dash https://orcid.org/0000-0001-7267-6104
Devjani Banerjee https://orcid.org/0000-0002-4287-2398
Aliasgar Vohra https://orcid.org/0000-0002-4845-084X
Ranjitsinh Devkar https://orcid.org/0000-0002-9863-7418
Debjani Chakraborty https://orcid.org/0000-0001-5871-4784

REFERENCES

[1] C. Roder, M. Thomson, *Drugs R&D* **2015**, *15*, 13.
[2] B. Bosco, A. Defant, A. Messina, T. Incitti, D. Sighel, A. Bozza, Y. Ciribilli, A. Inga, S. Casarosa, I. Mancini, *Molecules* **2018**, *23*, 1996.
[3] Y. Y. Huang, L. Y. Wang, C. H. Chang, Y. H. Kuo, F. F. Wong, *Tetrahedron* **2012**, *68*, 9658.
[4] S. Mert, A. S. Yağlıoğlu, I. Demirtas, R. Kasımoğulları, *Med. Chem. Res.* **2014**, *23*, 1278.
[5] L. D. Via, A. M. Marini, S. Salerno, C. L. Motta, A. Toninello, *Bioorg. Med. Chem.* **2009**, *17*, 326.
[6] G. M. Nitulescu, C. Draghici, A. V. Missir, *Eur. J. Med. Chem.* **2010**, *45*, 4914.
[7] S. Alyar, N. Özbek, N. O. İskeleli, N. Karacan, *Med. Chem. Res.* **2013**, *22*, 2061.
[8] S. U. Rai, A. M. Isloor, P. Shetty, K. S. R. Pai, H. K. Fun, *Arabian J. Chem.* **2015**, *8*, 317.
[9] A. Ansari, A. Ali, A. M. Shamsuzzaman, *New J. Chem.* **2017**, *41*, 16.
[10] K. Karrouchi, S. Radi, Y. Ramli, J. Taoufik, Y. N. Mabkhot, F. A. Al-aizari, M. Ansar, *Molecules* **2018**, *23*, 134.
[11] N. P. Prajapati, H. D. Patel, *Synth. Commun.* **2019**, *49*, 2767.
[12] O. Dömötör, M. A. Kiss, G. T. Gál, N. V. May, G. Spengler, M. Nové, A. C. Gašparović, E. Frank, E. A. Enyedy, *J. Inorg. Biochem.* **2020**, *202*, 110883.
[13] A. Sirbu, O. Palamarciuc, M. V. Babak, J. M. Lim, K. Ohui, E. A. Enyedy, D. S. Shova, D. Darvasiová, P. Rapta, W. H. Ang, V. B. Arion, *Dalton Trans.* **2017**, *46*, 3833.
[14] C. S. Allardyce, A. Dorcier, C. Scolaro, P. J. Dyson, *Appl. Organomet. Chem.* **2005**, *19*, 1.
[15] J. García-Tojal, A. García-Orad, J. L. Serra, J. L. Pizarro, L. Lezama, M. I. Arriortua, T. Rojo, J. Inorg, *Biochemistry* **1999**, *75*, 45.
[16] D. X. West, A. E. Liberta, S. B. Padhye, R. C. Chikate, P. B. Sonawae, A. S. Kumbhar, R. G. Yerande, *Coord. Chem. Rev.* **1993**, *123*, 49.
[17] F. A. Bechford, G. Leblanc, J. Thessing, M. Shaloski Jr., B. J. Frost, L. Li, N. P. Seeram, *Inorg. Chem. Commun.* **2009**, *12*, 1094.
[18] R. Pettinari, F. Marchetti, C. Di Nicola, C. Pettinari, A. Galindo, R. Petrelli, L. Cappellacci, M. Cuccioloni, L. Bonfili, A. M. Eleuteri, M. F. C. Guedes da Silva, A. J. L. Pombeiro, *Inorg. Chem.* **2018**, *57*, 14123.
[19] E. Păunescu, M. Soudani, P. Martin, R. Scopelliti, M. Lo Bello, P. J. Dyson, *Organometallics* **2017**, *36*, 3313.
[20] M. Muralisankar, R. Dheepika, J. Haribabu, C. Balachandran, S. Aoki, N. S. P. Bhuvanesh, S. Nagarajan, *ACS Omega* **2019**, *4*, 11712.
[21] M. Fabre, J. Jaud, M. Hliwa, J. P. Launay, J. Bonvoisin, *Inorg. Chem.* **2006**, *45*, 9332.
[22] J. Honorato, K. M. Oliveira, C. M. Leite, L. Colina-Vegas, J. A. Nóbrega, E. E. Castellano, J. Ellena, R. S. Correa, A. A. Batista, *J. Braz. Chem. Soc.* **2020**, *31*, 2237.
[23] M. A. Bennett, A. K. Smith, *J. Chem. Soc. Dalton Trans.* **1974**, 233.
[24] M. A. Bennett, T. N. Huang, T. W. Matheson, A. K. Smith, S. Ittel, W. Nickerson, *Inorg. Synth.* **1982**, *21*, 74.
[25] H. D. Patel, S. M. Divatia, E. D. Clercq, *Indian J. Chem.* **2013**, *52*, 535.
[26] R. N. Patel, N. Singh, K. K. Shukla, U. K. Chauhan, *Spectrochim. Acta A* **2005**, *61*, 287.
[27] a) A. D. Becke, *Phys. Re. A* **1988**, *38*, 3098; b) J. P. Perdew, *Phys. Re. B* **1986**, *33*, 8822.
[28] A. Schäfer, H. Horn, R. J. Ahlrichs, *Chem. Phys.* **1992**, *97*, 2571.
[29] C. Hättig, G. Schmitz, J. Koßmann, *Phys. Chem. Chem. Phys.* **2012**, *14*, 6549.
[30] R. Ahlrichs, M. Bar, M. Häser, H. Horn, C. Kölmel, *Chem. Phys. Lett.* **1989**, *162*, 165.
[31] K. Eichkorn, O. Treutler, H. Öhm, M. Haser, R. Ahlrichs, *Chem. Phys. Lett.* **1995**, *240*, 283.
[32] M. Sierka, A. Hogekamp, R. Ahlrichs, *J. Chem. Phys.* **2003**, *118*, 9136.
[33] a) J. Hepburn, G. Scoles, R. Penco, *Chem. Phys. Lett.* **1975**, *36*, 451; b) S. Grimme, J. Antony, S. Ehrlich, H. Krieg, *J. Chem. Phys.* **2010**, *132*, 154104.
[34] A. Klamt, G. Schuurmann, *J. Chem. Soc. Perkin Trans.* **1993**, *2*, 799.
[35] C. F. Macrae, P. R. Edgington, P. McCabe, E. Pidcock, G. P. Shields, R. Taylor, M. Towler, J. Van de Streek, *J. Appl. Cryst.* **2006**, *39*, 453.
[36] a) E. Runge, E. K. U. Gross, *Phys. Rev. Lett.* **1984**, *52*, 997; b) C. Adamo, D. Jacquemin, *Chem. Soc. Rev.* **2013**, *42*, 845.
[37] M. J. Frisch, G. W. Trucks, H. B. Schlegel, G. E. Scuseria, M. A. Robb, J. R. Cheeseman, *Gaussian 09, Rev D.1*, Gaussian, Inc, Wallingford CT **2013**.
[38] a) T. Yanai, D. P. Tew, N. C. Handy, *Chem. Phys. Lett.* **2004**, *393*, 51; b) J. O. F. Thompson, L. B. Klein, T. I. Sølling, M. J. Paterson, D. Townsend, *Chem. Sci.* **2016**, *7*, 1826; c) M. D. J. Waters, A. B. Skov, M. A. B. Larsen, C. M. Clausen, P. M. Weber, T. I. Sølling, *Phys. Chem. Chem. Phys.* **2019**, *21*, 2283.

[39] M. Cossi, N. Rega, G. Scalmani, V. Barone, *J. Comput. Chem.* **2003**, *24*, 669.
[40] M. N. Patel, C. R. Patel, H. N. Joshi, K. P. Thakor, *Spectrochim. Acta A* **2014**, *127*, 261.
[41] A. Tarushi, K. Lafazanis, J. Kljun, I. Turel, A. A. Pantazaki, G. Psomas, D. P. Kessissoglou, *J. Inorg. Biochem.* **2013**, *121*, 53.
[42] T. Mosmann, *J. Immunol. Methods* **1983**, *65*, 55.
[43] I. Ali, W. A. Wani, K. Saleem, *Synth. React. Inorg., Met.-Org., Nano-Met. Chem.* **2013**, *43*, 1162.
[44] R. Pulipaka, S. R. Dash, P. Khanvilkar, S. S. Jana, R. V. Devkar, D. Chakraborty, *Trans. Met. Chem.* **2019**, *38*, 603.
[45] X. M. Liu, L. H. Xie, J. B. Lin, R. B. Lin, J. P. Zhang, X. M. Chen, *Dalton Trans.* **2011**, *40*, 8549.
[46] L. N. Zhu, L. Yi, W. Dong, W. Z. Wang, Z. Q. Liu, Q. M. Wang, D. Z. Liao, Z. H. Jiang, S. P. Yan, *J. Coord. Chem.* **2006**, *59*, 457.
[47] T. Ya-Wen, C. Yun-Fan, L. Yong-Jie, C. Kuan-Hung, C. H. Lin, H. Jui-Hsien, *Molecules* **2018**, *23*, 59.
[48] A. A. Adebayo, P. A. Ajibade, *J. Chem.* **2016**, *15*, 3672062.
[49] P. Kumar, S. Dasari, A. K. Patra, *Eur. J. Med. Chem.* **2017**, *136*, 52.
[50] S. Thota, D. A. Rodrigues, D. C. Crans, E. J. Barreir, *J. Med. Chem.* **2018**, *61*, 5805.
[51] A. M. Pyle, J. P. Rehmann, R. Meshoyrer, C. V. Kumar, N. J. Turro, J. K. Barton, *J. Am. Chem. Soc.* **1989**, *111*, 3051.
[52] Y. C. Huang, J. Haribabu, C. M. Chien, G. Sabapathi, C. K. Chou, R. Karvembu, P. Venuvanalingam, W. M. Ching, M. L. Tsai, S. C. N. Hsu, *J. Inorg. Biochem.* **2019**, *194*, 74.
[53] J. Haribabu, G. Sabapathi, M. M. Tamizh, C. Balachandran, N. S. P. Bhuvanesh, P. Venuvanalingam, R. Karvembu, *Organometallics* **2018**, *37*, 1242.
[54] G. Kalaiarasi, S. Dharani, S. R. J. Rajkumar, V. M. Lynch, R. Prabhakaran, *J. Inorg. Biochem.* **2020**, *211*, 111176.
[55] A. Bouskila, E. Amouyal, C. Verchere-Beaur, I. Sasaki, A. Gaudemer, *J. Photochem. Photobiol. B. Biol.* **2004**, *76*, 69.
[56] R. Mudavath, B. Ushaiah, C. K. Prasad, K. Sudeepa, P. Ravindar, S. N. T. Sunitha, C. S. Devi, *J. Biomol. Struct. Dyn.* **2020**, *38*, 2849.
[57] H. Laila, A. Rahman, M. Rafat, E. I. Khatib, L. A. B. Nassr, A. M. Abu-Dief, M. Ismael, A. A. Seleem, *Spectrochim. Acta A* **2014**, *117*, 366.
[58] J. R. Lakowicz, G. Weber, *Biochemistry* **1973**, *12*, 4161.
[59] K. N. A. Rahman, J. Haribabu, C. Balachandran, N. S. P. Bhuvanesh, R. Karvembu, A. Sreekanth, *Polyhedron* **2017**, *135*, 35.
[60] T. K. Goswami, B. V. S. K. Chakravarthi, M. Roy, A. A. Karande, A. R. Chakravarty, *Inorg. Chem.* **2011**, *50*, 8452.
[61] M. Anjomshoa, S. J. Fatemi, M. Torkzadeh-Mahani, H. Hadadzadeh, *Spectrochim. Acta Part. A.* **2014**, *127*, 511.
[62] *ACD/ChemSketch, version 2020.1.2*, Advanced Chemistry Development, Inc, Toronto, ON, Canada, http://www.acdlabs.com **2020**.
[63] M. Thompson, ArgusLab 4.0.1., Planaria software LLC, Seattle, Wash, USA, **2004**.
[64] A. Hafeez, Z. S. Saify, A. Naz, F. Yasmin, N. Akhtar, *J. Comput. Med.* **2013**, 312183.
[65] S. Salentin, S. Schreiber, V. J. Haupt, M. F. Adasme, M. Schroeder, *Nucleic Acids Res.* **2015**, *43*, W443.
[66] N. Zaidi, E. Ahmad, M. Rehan, G. Rabbani, M. R. Ajmal, Y. Zaidi, *J. Phys. Chem. B* **2013**, *117*, 2595.
[67] G. Sudlow, D. J. Birkett, D. N. Wade, *Mol. Pharmacol.* **1976**, *12*, 1052.
[68] K. Zheng, F. Liu, X. M. Xu, Y. T. Li, Z. Y. Wu, W. Yan, *New J. Chem.* **2014**, *38*, 2964.
[69] A. Daina, V. Zoete, *Chem Med Chem.* **2016**, *11*, 1117.
[70] A. Daina, O. Michirlin, V. Zoete, *Sci. Rep.* **2017**, *7*, 42717.

SUPPORTING INFORMATION

Additional supporting information may be found online in the Supporting Information section at the end of this article.

How to cite this article: P. Khanvilkar, S. R. Dash, D. Banerjee, A. Vohra, R. Devkar, D. Chakraborty, *Appl Organomet Chem* **2021**, e6343. https://doi.org/10.1002/aoc.6343